

2023

A Novel Convolutional Neural Network Based on Combined Features from Different Transformations for Brain Tumor Diagnosis

Basant S. Abd El-Wahab,

Follow this and additional works at: <https://digitalcommons.aaru.edu.jo/erjeng>

Recommended Citation

S. Abd El-Wahab,, Basant (2023) "A Novel Convolutional Neural Network Based on Combined Features from Different Transformations for Brain Tumor Diagnosis," *Journal of Engineering Research*: Vol. 7: Iss. 2, Article 50.

Available at: <https://digitalcommons.aaru.edu.jo/erjeng/vol7/iss2/50>

This Article is brought to you for free and open access by Arab Journals Platform. It has been accepted for inclusion in Journal of Engineering Research by an authorized editor. The journal is hosted on [Digital Commons](#), an Elsevier platform. For more information, please contact rakan@aar.edu.jo, marah@aar.edu.jo, u.murad@aar.edu.jo.

A Novel Convolutional Neural Network Based on Combined Features from Different Transformations for Brain Tumor Diagnosis

Basant S. Abd El-Wahab*, Mohamed E. Nasr, Salah Khamis, Amira S. Ashour

Department of Electronics and Electrical Communications Engineering, Faculty of Engineering, Tanta University, Tanta, Egypt.

E-mail(s): basant_samir@f-eng.tanta.edu.edu, mohamed.nasr@f-eng.tanta.edu.eg, salah.khamis@f-eng.tanta.edu.eg, Amira.salah@f-eng.tanta.edu.eg, amirasashour@yahoo.com

Abstract- Brain tumors are a leading cause of death worldwide. With the advancements in medicine and deep learning technologies, the dependency on manual classification-based diagnosis drives down owing to their inaccurate diagnosis and prognosis. Accordingly, there is a clear need for a fully automated system to detect brain tumors. Deep learning models could generalize across diverse data sets; thus, we have turned to this technology to address the problem. The proposed model provides an accurate multi-class classification model for brain tumor using the convolution neural network (CNN) as a backbone. Our novel model is based on concatenating the extracted features from the proposed three branches of CNN, where each branch is fed by the output of different transform domains of the original magnetic resonance image (MRI). These transformations include Discrete Cosine Transform (DCT), Discrete Wavelet Transform (DWT), and the time-domain of the original image. Then, the CNN is employed followed by a concatenation layer, flatten layer, and dense layer, before using the SoftMax layer. The proposed model was applied to the Figshare dataset of brain tumor which consists of three classes pituitary, glioma, and meningioma. The results proved the advantage of the proposed system which achieved a high mean performance over 5-fold cross-validation with 98.89% accuracy, 98.78% F1-score, 98.74% precision, 98.82% recall, and 99.44% specificity. The comparative study with well-known models, as well as the pre-trained CNN models, established the potential of the proposed model. This novel approach has the potential to significantly improve brain tumor classification accuracy. It enables a more comprehensive and objective analysis of brain tumors, leading to improved treatment decisions and better patient care.

Keywords- Multi-class classification; brain tumor; discrete wavelet transform; discrete cosine transform; convolution neural network.

I. INTRODUCTION

Medical diagnosis and treatment planning require the crucial task of classifying brain tumors. There are various ways to classify brain tumors, including by their cell location, origin, grade, and histology. Brain tumors can be regarded as based on the cell source as primary or secondary tumors [1-3]. Other categorization can be considered based on the tumor histology, including glioma, meningioma, pituitary adenomas, and others [4-6]. Among these, Glioma is a type of brain tumor that begins in the glial cells that nourish and assist cells of nerve in the

brain. They are the most prevalent primary brain tumor and can be categorized as low-grade or high-grade. Low-grade gliomas have a slower growth rate and a better prognosis, whereas high-grade gliomas grow aggressively and rapidly. Meningioma on the other hand, are brain tumors that emerge from the meninges, the protective membranes that cover the brain and spinal cord. They usually grow slowly and tend to be benign, meaning they do not spread to other parts of the body. However, some meningioma can be malignant, requiring more aggressive treatment. Pituitary tumors arise in the pituitary gland, a small gland located at the base of the brain. This gland produces hormones that regulate various bodily functions, such as growth, metabolism, and reproductive function. Pituitary tumors can be either functional or non-functional, with functional tumors producing hormones and causing hormonal imbalances, while non-functional tumors do not produce hormones but can cause neurological symptoms by compressing the surrounding structures. The classification-based identification of brain tumors is necessary for patients. Different computer-aided diagnosis (CAD) systems were built to assist in the analysis of medical conditions. In the case of brain tumors, a CAD system can analyze imaging data from magnetic resonance imaging (MRI) to classify different types of brain tumors. By extracting various features from the tumor, such as size, texture, shape, and location, the CAD system can categorize the tumor into different groups, including glioma, meningioma, or pituitary tumors.

MRI is a frequently employed imaging technique for the classification of brain tumors that offers various benefits over alternative imaging methods. Among the advantages of MRI images in brain tumor classification are the following: Firstly, MRI provides high-resolution images of the brain that can uncover intricate details and structures that might be hard to discern with other imaging methods. Secondly, MRI permits imaging in multiple planes, such as sagittal, axial, and coronal planes, thereby allowing for a more comprehensive view of the tumor and its surrounding structures. Thirdly, MRI is a non-invasive imaging modality that does not employ ionizing radiation, rendering it less hazardous than other imaging techniques, such as CT scans. Finally, MRI can be conducted with contrast agents to enhance the visibility of the tumor and its surrounding structures.

The use of a CAD offers several advantages, including improved accuracy, consistency, time-saving, objective analysis, and early detection. The task of classifying brain tumors into subtypes presents significant challenges due to a couple of factors: i) brain tumors exhibit considerable variations in intensity, and shape [7] and ii) tumors from different uncontrolled types may have comparable presence [8]. Glioma, meningioma, and pituitary tumor are the most widespread brain tumors. Manual delineated tumor borders were applied for extracting the features from the area of interest for further classification using support vector machine (SVM) with bag of words (BoW). Afterward, Charron *et al.* [9] utilized a deep CNN for monitoring brain metastases. However, deep transfer learning has emerged as a dominant technique [10]. This approach involves using a pre-trained CNN that was originally improved for different applications. Transfer learning provided significant potential in the CAD system ability. In addition, Yang *et al.* [11] compared the performance of using AlexNet and GoogLeNet, where GoogLeNet proved its superiority. Meanwhile, Talo *et al.* [12] accomplished impressive classification performance by employing deep transfer learning. Their experimentation involved training modified dense layers, augmenting data during training, and fine-tuning a transfer learned model, all with the use of ResNet-34.

A. Related Work

Various classification models have been explored by different researchers in the brain tumor classification field. Anarki *et al.* [13] employed a CNN-based structure, attaining a classification accuracy of 94.2%. Gumaei *et al.* [14] combined Principal Component Analysis (PCA) with normalized GIST descriptors, using a regularized extreme learning machine for classification, and achieved an accuracy rate of 94.23%. Sajjad *et al.* [15] relied on a pre-trained VGG-19 model along with data augmentation to achieve an overall accuracy of 94.58%. In another study, Swati *et al.* [16] utilized pre-trained VGG19 models and implemented transfer learning and fine-tuning specifically for classifying brain tumors. This approach achieved an impressive accuracy of 94.82%.

In addition, Deepak *et al.* [17] proposed a different strategy by utilizing a pre-trained GoogleNet model with transfer learning and compared to SVM, Naive Bayes, Decision Tree, K-nearest Neighbor, and Linear Discrimination, leading to a high classification accuracy of 97.1%. Ishayaji *et al.* [18] introduced a classification model that combined two paths from CNN structures, utilizing Bayesian optimization. This innovative approach yielded a remarkable accuracy of 97.37%. Kakarla *et al.* [19] focused on the design of the CNN structure itself and employed eight layers, resulting in a classification accuracy of 97.42%. Kumar *et al.* [20] established a pre-trained ResNet-50 model for classification and incorporated average pooling and Softmax layers into the output layer, achieving the highest accuracy of 97.48%. A classification system was

implemented by Ismael *et al.* [21] using extracted features by Gabor filter and DWT for training a multi-layer perceptron. To create the training and validation sets, the database images were randomly divided into 70% and 30%, respectively. This approach achieved a high accuracy of 91.9%. Meanwhile, Abiwinanda *et al.* [22] applied a CNN-based deep learning system to classify brain tumors without prior segmentation of the tumor regions. The CNN architecture was designed with five learnable layers, each layer uses 3x3 filters, and accomplished a classification accuracy of 81%. However, the model had limitations in discriminating between meningioma and pituitary tumors. To enhance the diagnosis accuracy, the CNN features were combined with an extreme learning machine (ELM) classifier.

For brain tumor classification, a capsule network (CapsNet) was designed by Afshar *et al.* [23]. Also, Afshar *et al.* [24] proposed the CapsNets for extracting 64 feature maps with achieving 86.56% accuracy. Abir *et al.* [25] managed a classification based on the gray level co-occurrence matrix (GLCM) with probabilistic neural network (PNN) for final classification. It achieved maximum accuracy of 83.33%. Chattopadhyay *et al.* [26] utilized a DL approach to detect brain tumors from MRI images. Despite achieving a remarkable accuracy rate of 99.74%, the study only considered two labels in their database, namely tumor and non-tumor. Haq *et al.* [27] put forth a robust DL- classification method for enhancing the performance.

From the preceding studies, it is noted that using different transform domains provides significant features for accurate diagnosis. In addition, for classifying brain tumors as meningioma, glioma, and pituitary tumors, several limitations encountered the designed systems, including i) the performance of existing methods is insufficient, ii) the previous techniques relied on manual identification of tumor regions before classification, which hindered full automation, iii) and the use of CNNs and their variations achieved limited improvement in the diagnosis performance. To overcome these limitations, this paper presents a multi-class classification system that is automatic and accurate in identifying pituitary, meningioma, and glioma. This study proposes a novel approach that integrates artificial intelligence and multi-omics data to improve brain tumor classification accuracy, allowing for more precise diagnoses and personalized treatment strategies. The proposed model includes three parallel branches of the CNN layers and applied different transform domains on the input before each branch. To extract the features vector, CNN was applied after each of the different domains to take the benefit of various resolution from the input MRI images. Accordingly, we can summarize the contributions of the proposed model include more efficient and accurate classification system for brain tumor CAD applications, as follows:

- 1- Carrying out the benefits of the discrete cosine transform that offers many advantages such as: energy compaction properties, resistance to data loss, real-valued inputs and

- outputs and ease of implementation.
- 2- Performing the advantage of DWT, which is powerful due to its multiresolution analysis, excellent time-frequency localization, fast algorithm, and robustness.
 - 3- Achieving effective performance compared to the conventional CNN network and well-known models.
 - 4- Giving a significantly efficient performance.

The organization of this paper is as follows: section 2 provides description of the dataset utilized and a framework of the proposed model. Section 3 presents the experiments, the evaluation results, and a discussion of the outcomes. Finally, section 4 concludes the paper.

II. METHODOLOGY

The proposed model presented a new structure from CNN layer based on combining three branches from various transform domains like time domain of MRI input images, images in DWT and images in DCT. The combination feature vector was then classified by Softmax layer. The proposed model performance was examined by applying the five-fold cross validation to produce mean evaluation metrics over five folds.

A. Dataset

A publicly available Figshare dataset of brain tumors was utilized that comprises 3,064 MRI slices of the brain which is contrast-enhanced T1-weighted MR images, collected from 233 patients, and encompasses three types of brain tumors: 930 slices pituitary, 1426 slices glioma, and 708 slices meningioma, viewed from three distinct perspectives: sagittal, axial, and coronal. The dataset is provided in each MAT-file containing a structure that includes patient identification which labeled by radiologists according to the tumor type [28].

B. Convolutional Neural Network

A deep CNN [29] is made up of multiple interconnected layers of nodes that are intended to learn and extract increasingly complex characteristics from an input image. Typically, the initial layer of a CNN is a convolutional layer, which applies a set of filters that can be learned to the input image. These filters scan the entire image and create a feature map that indicates the presence of a particular feature or pattern in various parts of the image. The initial convolutional layer's output then passes through a non-linear activation function, such as the rectified linear unit (ReLU), which introduces non-linearity into the network and facilitates the acquisition of more intricate representations. The output of convolution layer followed by ReLU activation function can be represented as follow [30]:

$$C_{i,j,k} = \sum_{l=1}^L \sum_{m=1}^M \sum_{n=1}^N I_{i+l-1,j+m-1} \times F_{l,m,c,k} \quad (1)$$

$$O_{i,j,k} = \max(0, C_{i,j,k}) \quad (2)$$

where C, I and F are the output, input and filter of convolution layer, respectively, also, L, M, and N are the dimensions of the filter, while, c and k are the indices of the input and output channels, respectively, and O is the output after activation function.

The successive layers of the CNN usually alternate between convolutional/pooling layers. Pooling layers drive down the dimensionality and improve the network's robustness against variations. The output of the average pooling layer can be represented as follow [31]

$$P_{i,j,k} = \frac{1}{L_p \times M_p} \sum_{l=1}^{L_p} \sum_{m=1}^{M_p} X_{i \times s + l - 1, j \times s + m - 1, k} \quad (3)$$

where P is the output of the average pooling layer, X is the input. L_p , M_p , s and k are the dimensions of the pooling window, the stride, the channel index, respectively.

Usually, the concluding layers of a CNN consist of fully connected layers that employ the previously extracted high-level features to predict the input image's characteristics. Afterward, a Softmax activation function is frequently employed, which generates the distribution of a probability over the potential output categories. The output of the fully connected layer and Softmax layer can be represented as follow [32] :

$$Y_k = \sum_{i=1}^N I_i \times W_{i,k} + b_k \quad (4)$$

$$O_k = \frac{e^{z_k}}{\sum_{i=1}^K e^{z_i}} \quad (5)$$

where Y_k and I are the output and the input vectors for the fully connected layer, respectively. W, b, N, and k are the weight matrix, the bias vector, the number of neurons in the previous layer, and the index of the neuron in the current layer, respectively. Also, O_k and z are the output vector of class probabilities and the input vector of scores, respectively. K is the total classes number.

C. Discrete Wavelet Transform

The DWT breaks down the image into numerous frequency sub-bands as shown in figure 1 that offer varying degrees of detail. It utilizes a set of filters called wavelets. The low-frequency components provide an overview of the patterns or trends within the signal, while the high-frequency components reveal signal details. DWT has good time-frequency localization, making it capable of precisely identifying signal changes at a specific time and frequency, which is useful in the medical diagnosis. DWT is also robust and can handle signals with non-stationary behavior, making it a useful tool in analyzing complex signals. Among the wavelet functions, the Daubechies wavelets are the most popular due to their compact support and excellent time-frequency localization.

Approximation Image (LL)	Horizontal detail (HL)
Vertical detail (LH)	Diagonal detail (HH)

Figure 1. Wavelet sub-bands for the image after DWT.

The DWT can be expressed as follow [33]:

$$W_{j,k} = \sum_n x_n \cdot \Psi_{j,k}(n) \quad (6)$$

$$H_{j,k} = \sum_n h_n \cdot x_{2n-k} \cdot 2^{-j/2} \quad (7)$$

$$L_{j,k} = \sum_n l_n \cdot x_{2n-k} \cdot 2^{-j/2} \quad (8)$$

where x_n is the input signal, j and k are integer parameters that specify the scale and translation of the wavelet function and W is the wavelet coefficient at scale j and translation k .

D. Discrete Cosine Transform

The Discrete Cosine Transform (DCT) converts a series of data points into a set of cosine functions of different frequencies, which are useful for analyzing the spectral content of the original image by eliminating extraneous information. Unlike the Discrete Fourier Transform (DFT), which uses complex inputs and outputs, the DCT uses only real-valued inputs and outputs, making it faster and more efficient. The DCT is computed by multiplying the input signal by a set of cosine functions with varying frequencies and amplitudes, then summing the products. The resulting coefficients represent the frequency components of the input signal. The DCT has excellent energy compaction qualities that allow it to represent the image using fewer coefficients without sacrificing significant information. The DCT can be computed as follow [34]:

$$X[k] = \sqrt{(2/N)} \sum_0^{N-1} x[n] \times \cos((\pi/N) \times (n + 1/2) \times k) \quad (9)$$

where $x[n]$ represents the input signal, $X[k]$ represents the DCT coefficients for $k=0, 1, \dots, N-1$, and N is the length of the signal. Compared to other signal processing techniques, the DCT offers several benefits. Some of the main advantages of DCT are:

- **Energy compaction:** DCT's superior energy compaction properties allow it to pack most of the signal energy into a few coefficients.
- **Robustness to data loss:** DCT is resistant to data loss, making it helpful in situations where the input data is

incomplete or noisy.

- **Real-valued inputs and outputs:** Since DCT only uses real-valued inputs and outputs, it's faster and more efficient than other transform methods like the Fourier Transform. This feature also makes DCT suitable for hardware implementation, such as digital signal processors.
- **Easy implementation:** DCT is straightforward to implement and widely available in software libraries and hardware components. This property makes it accessible to developers and researchers who can leverage it to build new signal processing algorithms and applications.

E. The Proposed Model

The proposed model uses three branches from the CNN layer in various transform domains such as time domain, DWT and DCT with the 5-fold of cross-validation to achieve accurate and efficient multi-class classification. It consists of combining feature vectors from three branches of CNN structure layers. Each branch cascaded from two blocks from block 1 and one block from block 2, where **Block 1** includes (3×3,32) kernel convolution layer, (1×1,10) kernel convolution layer, (2×2) kernel average pooling, (1×1,10) kernel convolution layer. On the other hand, **Block 2** consists of (3×3,32) kernel convolution layer, (1×1,10) kernel convolution layer, (2×2) kernel average pooling.

The three CNN branches produced feature vectors such as feature vector F_t from direct MRI images, feature vector F_c from MRI images in DCT domain and feature vector F_w from MRI images in DWT domain. Then, the total feature vector F_T obtained by combining the three outputs from the three branches by Concatenate layer as follow:

$$F_t = \begin{bmatrix} f_{t111} & \dots & f_{t1n1} \\ \vdots & \ddots & \vdots \\ f_{tm11} & \dots & f_{tmn1} \end{bmatrix}_{m \times n \times 1} \cdot \begin{bmatrix} f_{t11p} & \dots & f_{t1np} \\ \vdots & \ddots & \vdots \\ f_{tm1p} & \dots & f_{tmnp} \end{bmatrix}_{m \times n \times p} \quad (10)$$

$$F_c = \begin{bmatrix} f_{c111} & \dots & f_{c1n1} \\ \vdots & \ddots & \vdots \\ f_{cm11} & \dots & f_{cmn1} \end{bmatrix}_{m \times n \times 1} \cdot \begin{bmatrix} f_{c11p} & \dots & f_{c1np} \\ \vdots & \ddots & \vdots \\ f_{cm1p} & \dots & f_{cmnp} \end{bmatrix}_{m \times n \times p} \quad (11)$$

$$F_w = \begin{bmatrix} f_{w111} & \dots & f_{w1n1} \\ \vdots & \ddots & \vdots \\ f_{wm11} & \dots & f_{wmn1} \end{bmatrix}_{m \times n \times 1} \cdot \begin{bmatrix} f_{w11p} & \dots & f_{w1np} \\ \vdots & \ddots & \vdots \\ f_{wm1p} & \dots & f_{wmnp} \end{bmatrix}_{m \times n \times p} \quad (12)$$

$$F_T = \text{Concatenate}([F_t F_c F_w]) \quad (13)$$

where f_{tmnp} , f_{cmnp} and f_{wmnp} are the features in the feature vectors in the time domain, DCT domain and DWT domain, respectively. Likewise, m, n and p indicate the dimension (height, width and depth or channel number) of the feature vector produced from each branch. After that the total feature vector applied to fully connected layer, dense layer and Softmax layer for classification. Table 1 demonstrates the proposed model structure in detail. Figure 2 displays the block diagram of proposed model framework.

The proposed model structure implements a five-fold cross-validation approach to determine the mean performance of the model. During training, in the first branch the training images directly utilized to train the model. But the second branch and third branch, the input MRI images transformed into DCT and DWT domain, respectively. At the beginning of training, weights of the model were randomly initialized, and then in each epoch the model was trained.

F. Evaluation metrics

Various methods exist to demonstrate the efficacy of classification outcomes. To evaluate our results, we have

focused on four primary criteria, namely accuracy, F1-score, precision, recall, and specificity. The measure of the overall correctness of a multi-class classification model is accuracy. It is computed as the ratio of correct estimates to the total number of estimates generated by the model. The F1-score assesses the accuracy of a multi-class classification model by merging precision and recall for each class. It is the weighted harmonic mean of precision and recall for all classes. A higher F1-score indicates a more balanced precision-recall trade-off for all classes.

While the precision assesses the fraction of pertinent outcomes among the total number of results predicted by a multi-class classification model for each class. It is calculated as the ratio of true positive predictions to the sum of true positive and false positive predictions for each class. Recall evaluates the capability of a multi-class classification model to accurately detect significant outcomes for each class. Specificity measures a multi-class classification model's accuracy in correctly identifying negative instances for each class.

Table 1. The detailed configuration for the proposed model.

Layer	Filter number	Kernal size	Output shape	Parameter
The layers in Each branch				
Input Layer	–	–	(254,254,1)	0
Conv2D	32	3×3	(252,252,32)	320
Conv2D	10	1×1	(252,252,10)	330
AveragePooling2D	–	2×2	(126,126,10)	0
Conv2D	10	1×1	(126,126,10)	110
Conv2D	32	3×3	(124,124,32)	2912
Conv2D	10	1×1	(124,124,10)	330
AveragePooling2D	–	2×2	(62,62,10)	0
Conv2D	10	1×1	(62,62,10)	110
Conv2D	32	3×3	(60,60,32)	2912
Conv2D	10	1×1	(60,60,10)	330
AveragePooling2D	–	2×2	(30,30,10)	0
Concatenate				
Concatenate	–	–	(30,30,30)	0
Flatten	–	–	27000	0
Dense	–	–	256	6912256
Dense (Softmax)	–	–	3	771

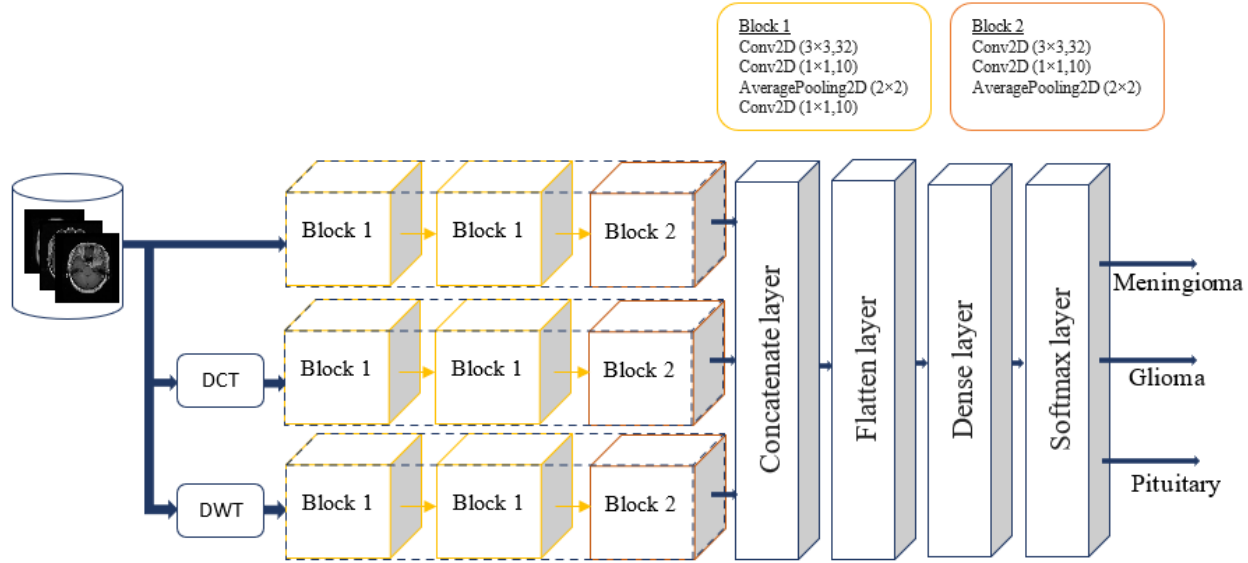


Figure 2. The proposed model for multi-class brain classification.

The equations for these metrics as follow [35]:

$$Accuracy = \frac{TP + TN}{TP + FP + FN + TN} \quad (14)$$

$$Recall = \frac{TP}{TP + FN} \quad (15)$$

$$Precision = \frac{TP}{TP + FP} \quad (16)$$

$$F1 - score = 2 \times \frac{Recall \times Precision}{Recall + Precision} \quad (17)$$

$$Specificity = \frac{TN}{TN + FP} \quad (18)$$

where TP, TN, FP and FN are the true positive, true negative, false positive, and false negative values, respectively.

III. RESULTS AND DISCUSSION

The proposed model was developed using Python and TensorFlow, which are offered by Google Colab services. To speed up convergence, we used Adam optimizer, which accelerates gradient vectors in the correct direction. The model was compiled ten epochs number and sparse categorical cross-entropy loss was used to upgrade the weights during training. To analyze the proposed model, a five-fold cross-validation method was applied. Within each iteration, the dataset was disjointed into 80% for validation and training, and the residual 20% was used to compute the model's performance over five iterations.

Firstly in the proposed model, each individual branch was studied and evaluated if utilized as the model for brain

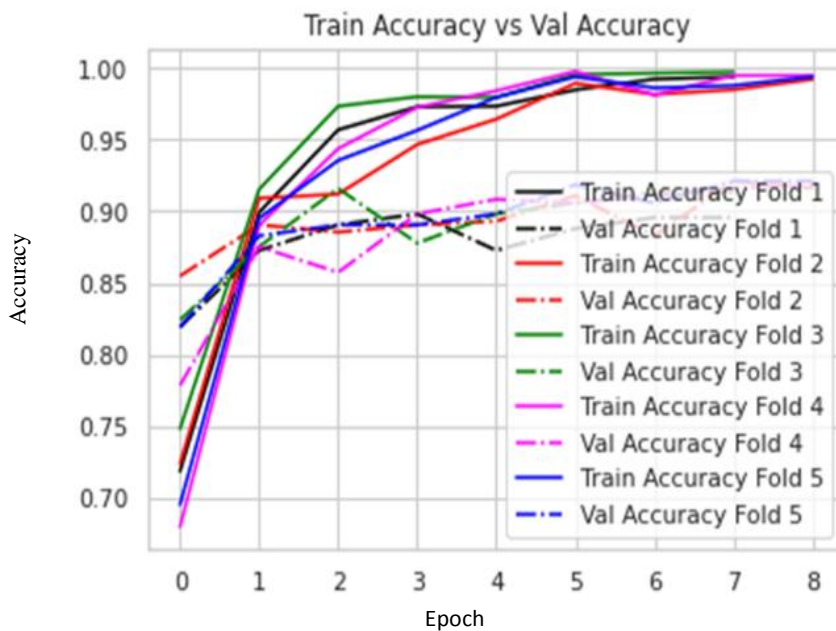
classification. Figure 3 describes the validation and training accuracy with each epoch for the model of the time domain, DWT or DCT branch utilized as model for brain classification. Furthermore, the evaluation metrics were computed for each branch in a different transform domain as the model for brain classification. Tables 2 to 4 demonstrate the performance of the different models in various transform domains.

Table 2. The performance evaluation for time domain model.

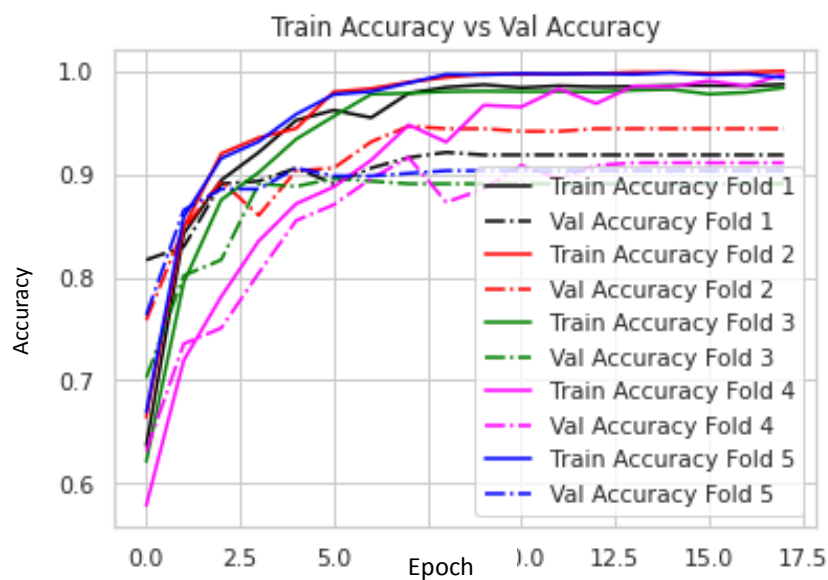
Fold	Accuracy %	Loss	F1-score %	Precision %	Recall %	Specificity %
1	92.82	0.24	91.75	92.39	91.26	96.11
2	93.64	0.21	93.11	92.81	93.43	96.75
3	92.82	0.26	92.15	92.39	91.92	96.19
4	92.66	0.28	91.49	91.61	91.41	96.08
5	93.46	0.22	92.52	93.15	92.03	96.56
Mean	93.08	0.24	92.21	92.47	92.01	96.34
SD	±0.39	±0.02	±0.57	±0.52	±0.77	±0.27

Table 3. The performance evaluation for DWT domain model.

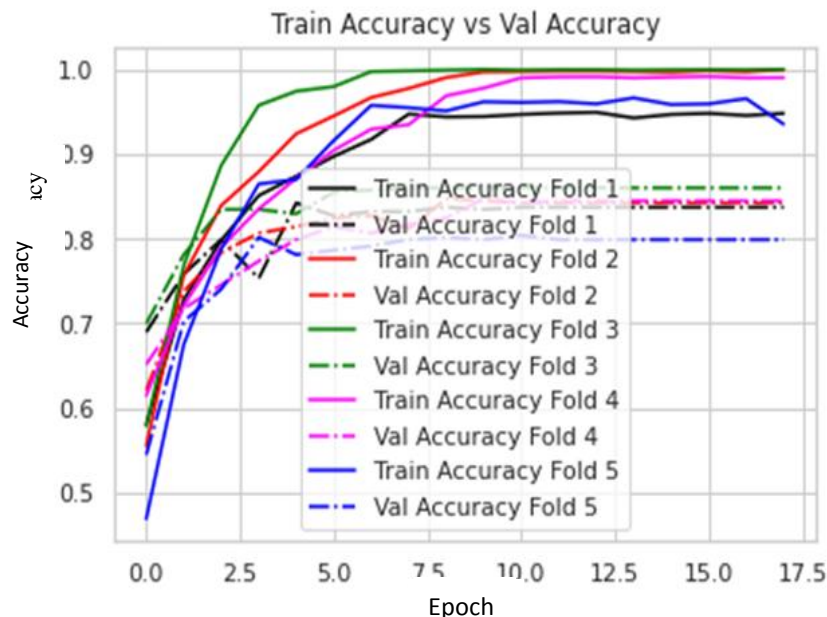
Fold	Accuracy %	Loss	F1-score %	Precision %	Recall %	Specificity %
1	92.82	0.19	91.59	91.43	91.78	96.29
2	92.99	0.20	91.98	92.03	91.94	96.42
3	86.62	0.42	85.45	85.61	85.88	93.16
4	92.49	0.22	91.54	91.36	91.77	96.19
5	92.16	0.20	91.49	91.44	91.56	95.99
Mean	91.42	0.25	90.41	90.37	90.59	95.61
SD	±2.41	±0.09	±2.49	±2.39	±2.36	±1.23



(a)



(b)



(c)

Figure 3. The training and validation accuracy with each epoch for different models in various domains, (a) time domain model, (b) DWT model, and (c) DCT model.

Table 4. The performance evaluation for DCT domain model.

Fold	Accuracy %	Loss	F1-score %	Precision %	Recall %	Specificity %
1	84.01	0.39	81.74	81.55	82.15	91.61
2	83.36	0.68	81.11	80.95	81.27	91.43
3	81.24	0.71	79.14	79.62	78.74	89.99
4	85.64	0.41	85.09	85.09	85.23	92.52
5	80.07	0.56	77.75	77.68	77.82	89.89
Mean	82.86	0.55	80.96	80.98	81.04	91.09
SD	±1.99	±0.13	±2.51	±2.45	±2.63	±1.01

Tables 2 through 4 reveal that the model in time domain obtained the best performance compared with the other models in DWT and DCT. The performance of the time model achieved 93.08%±0.39% accuracy, 92.21%±0.57% f1-score, 92.47%±0.52% precision, 92.01%±0.77% recall and 96.34%±0.27% specificity. while DWT and DCT models achieved accuracy 91.42%±2.41% and 82.86%±1.99%, respectively.

In this section, the proposed model performance was evaluated which combined between three branches in various domains. Table 5 evidence the proposed model performance with different metrics over five-fold cross validation. Table 5 indicates that the performance was increased by combining between the brain tumor MRI images in different domains. Due to performing combining the benefits of various transformations such as time domain, DCT, and DWT. where the DCT provides energy compaction properties, and DWT

provides multiresolution analysis and excellent time-frequency localization. Where the proposed model accuracy achieved 98.89%±0.44% which was the best result compared with the individual model in each domain.

Table 5. The proposed system performance.

Fold	Accuracy %	Loss	F1-score %	Precision %	Recall %	Specificity %
1	99.18	0.03	99.17	99.12	99.22	99.57
2	99.18	0.03	98.99	99.01	98.97	99.59
3	98.04	0.08	97.82	97.59	98.06	99.06
4	98.86	0.05	98.81	98.65	98.96	99.44
5	99.18	0.02	99.11	99.31	98.91	99.52
Mean	98.89	0.042	98.78	98.74	98.82	99.44
SD	±0.44	±0.02	±0.49	±0.61	±0.39	±0.19

Also, F-score, precision, recall and specificity of the proposed model achieved 98.78%±0.49%, 98.74%±0.61%, 98.82%±0.39%, 99.44%±0.19%. Table 6 shows the confusion matrix for the proposed model in each fold. Moreover, the detailed evaluation metrics for each class in a different fold were computed as illustrated in Table 7.

By examining the confusion matrix, the classification results for different types of tumors can be obtain in a highly detailed. Table 6 provides an exhaustive account of the confusion matrix for the proposed model, which was run for the fifth fold. Table 6 observes that 608, 608, 601, 606 and 608 tumor images were classified correctly in the 5-folds,

respectively. Meanwhile, the remaining 5, 5, 12, 7 and 5 images were classified inaccurately in the 5-fold respectively, leading to an overall classification accuracy of 99.18% 1-fold, 98.04% 2-fold, 98.86% 3-fold, 99.18% 4-fold and 99.18% 5-fold.

A. Comparative Study Between the Proposed Model and Traditional CNN Model

In this section the proposed model was compared with the other famous CNN network such as VGG16 [36], VGG19 [36], Inception V3 [37], ResNet50 [38], Efficient b0 [37], Efficient

b7, MobileNet [39], MobileNet V2 and MobileNet V3 small. Figure 4 demonstrates the comparative study by computing the evaluation metrics for each model.

Figure 4 describes that the proposed model outperformed the other CNN model, achieving the best result. Where VGG19 model was the best CNN model in accuracy metric which achieved 93.05%. Besides, MobileNet model was the best compared to with the other CNN models which achieved 89.16% F1-score.

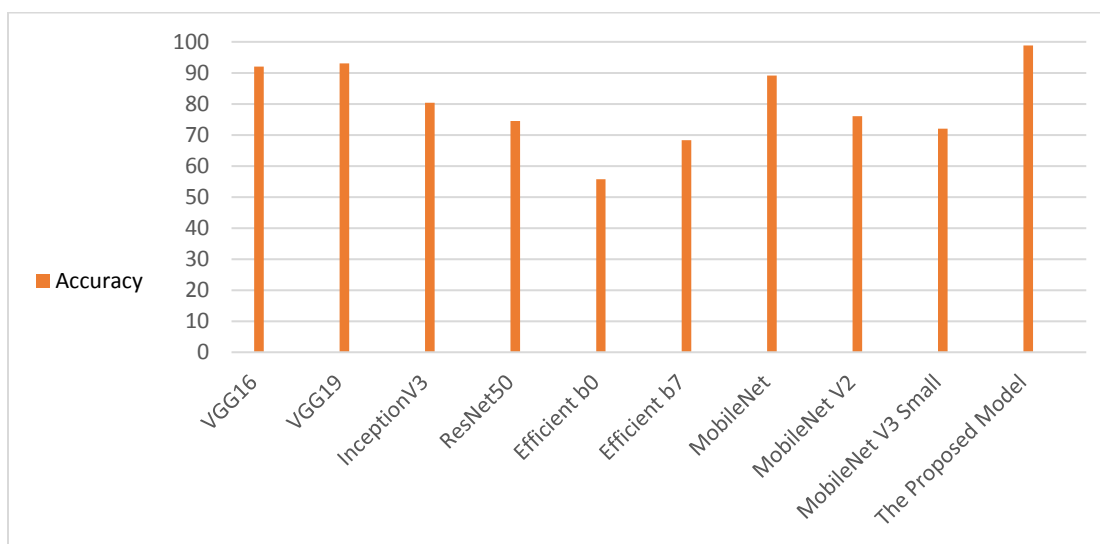
Table 6. the confusion matrix of the proposed model in each fold.

Class	Meningioma	Glioma	Pituitary
Fold 1			
Meningioma	150	2	0
Glioma	3	293	0
Pituitary	0	0	165
Fold 2			
Meningioma	121	1	2
Glioma	2	291	0
Pituitary	0	0	196
Fold 3			
Meningioma	133	1	3
Glioma	6	293	1
Pituitary	0	1	175
Fold 4			
Meningioma	145	2	0
Glioma	5	280	0
Pituitary	0	0	181
Fold 5			
Meningioma	122	2	1
Glioma	0	300	1
Pituitary	0	1	186

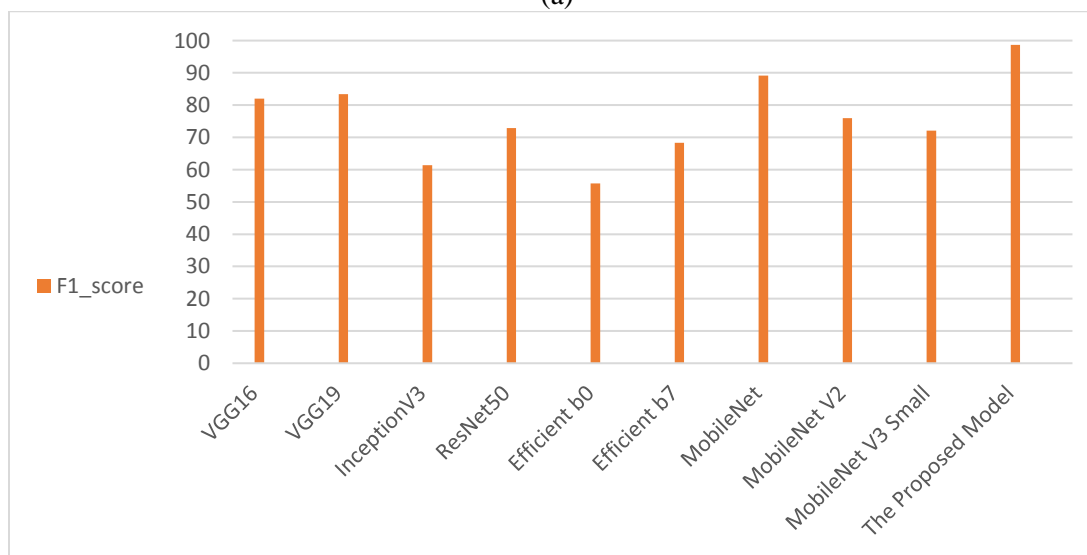
Table 7. The proposed model performance in each fold.

Class	F1-score%	Precision%	Recall%	Specificity%	Accuracy %
Fold 1					
Meningioma	98.36	98.04	98.68	99.35	99.18
Glioma	99.15	99.32	98.99	99.37	99.18
Pituitary	100	100	100	100	100
Fold 2					
Meningioma	97.98	98.37	97.58	99.59	99.18
Glioma	99.49	99.66	99.32	99.69	99.51
Pituitary	99.49	98.99	100	99.52	99.67
Fold 3					

Meningioma	96.38	95.68	97.08	98.74	98.37
Glioma	98.49	99.32	97.67	99.36	98.53
Pituitary	98.59	97.77	99.43	99.08	99.18
Fold 4					
Meningioma	97.64	96.67	98.64	98.93	98.86
Glioma	98.77	99.29	98.25	99.39	98.86
Pituitary	100	100	100	100	100
Fold 5					
Meningioma	98.79	100	97.61	100	99.51
Glioma	99.34	99.01	99.67	99.04	99.35
Pituitary	99.21	98.94	99.47	99.53	99.51



(a)



(b)

Figure 4. The calculated evaluation metrics resulted from the comparative study between proposed model and well-known CNN network. a) Accuracy valuation, and b) F1-score valuation.

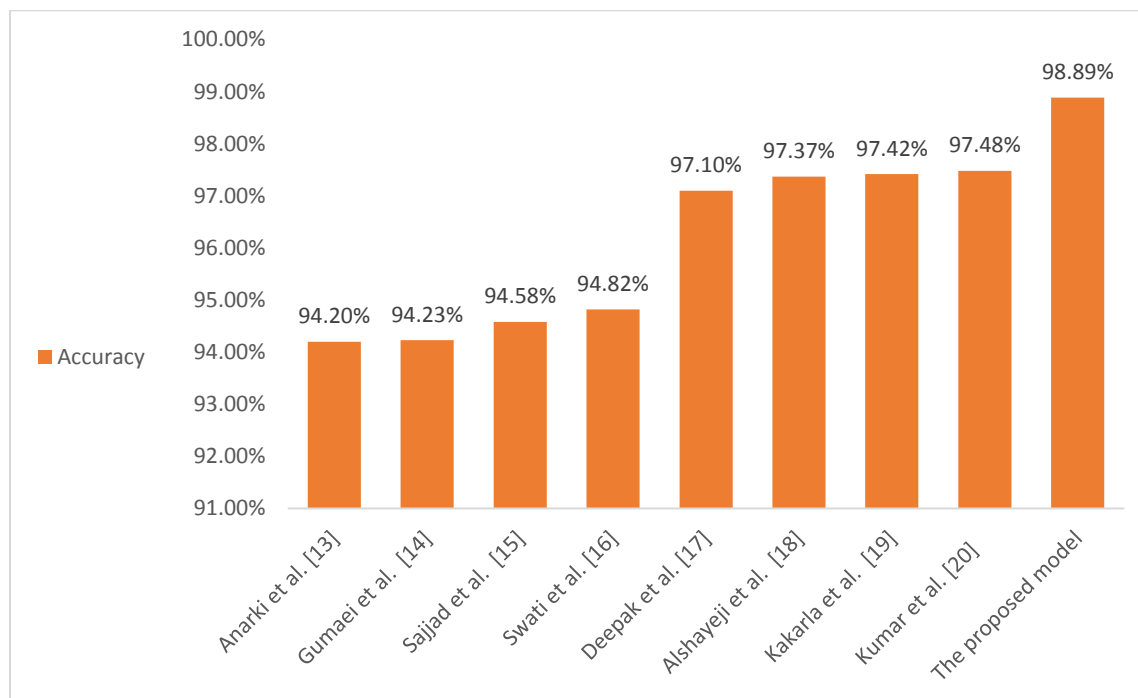


Figure 5. The comparative between the proposed model and state-of-the-art models.

B. Discussion

The proposed model we have suggested was evaluated against other recent concurrent models, such as those presented in Anarki *et al.* [13], Gumaei *et al.* [14], Sajjad *et al.* [15], Swati *et al.* [16], Deepak *et al.* [17], Alshayegi *et al.* [18], Kakarla *et al.* [19], Kumar *et al.* [20]. Figure 5 presents a comparison of our proposed model's accuracy percentage with these published models.

Figure 5 indicates that the proposed model has a high accuracy of 98.89%, surpassing the performance of the present models. Several studies have explored different techniques to classify brain tumors, Anarki *et al.* [13] utilized a classification model based on the CNN structure, achieving 94.2% classification accuracy. Gumaei *et al.* [14] applied a hybrid feature extraction technique, combining Principal Component Analysis (PCA) with normalized GIST descriptors, and used a regularized extreme learning machine for classification, resulting in a 94.23% accuracy rate. Sajjad *et al.* [15] utilized a pre-trained VGG-19 and data augmentation to achieve a 94.58% overall accuracy. Swati *et al.* [16] implemented by pre-trained VGG19 models which used transfer learning and fine-tuning for classifying brain tumor and achieved 94.82% accuracy.

Deepak *et al.* [17] proposed a pre-trained GoogleNet with the transfer learning with 97.1% classification accuracy. Alshayegi *et al.* [18] introduced classification model using combined two paths from CNNs structure with using Bayesian optimization. This approach achieved 97.37% accuracy. In Kakarla *et al.* [19] eight layers were used in designing a CNN structure, achieving

a classification accuracy of 97.42%. Kumar *et al.* [20] established a pre-trained ResNet-50 model for classification by inserting average pooling and Softmax layers in the output layer, achieving 97.48% accuracy.

IV. CONCLUSION

Brain tumors are an extremely severe condition that can greatly reduce a person's chances of survival. An incorrect diagnosis of a brain tumor can lead to confusion about the appropriate medical treatment, further reducing the patient's chance of recovery. Therefore, accurately detecting the presence of brain tumors is crucial for effective treatment planning and improving the overall quality of life for those with this disease. CNN networks are often recommended for the proper classification of brain tumors from MRI images.

The proposed model has undergone training using the Figshare dataset for multi-class classification. The benefits of MRI images in three different transform domains such as time, DCT and DWT domains have been utilized to obtain an accurate brain tumor classification model. The feature vector from MRI images in the proposed model was obtained by combining the feature vectors resulting from three branches from the CNN structure in different transform domains. Compared to the traditional CNN network and the state-of-the-art models, the system attained the highest classification accuracy. To assess the system's robustness, various metrics were used to evaluate its performance. Additionally, the system exhibited favorable performance even when trained with a limited number of samples.

The proposed brain tumor diagnosis system combined the benefits of the three transform domains to extract the features using the CNN network. It achieved the best performance compared to using the extracted features from a single domain. The results showed that the proposed model achieved 98.89% accuracy, 98.78% F1-score, 98.74% precision, 98.82% recall, and 99.44% specificity over 5-fold cross-validation.

Funding: The authors state that this research has not received any type of funding.

Conflicts of Interest: The authors declare that there is no conflict of interest.

REFERENCE

- [1] Neugut, A. I., Sackstein, P., Hillyer, G. C., Jacobson, J. S., Bruce, J., Lassman, A. B., & Stieg, P. A., “Magnetic Resonance Imaging-Based Screening for Asymptomatic Brain Tumors: A Review,” *Oncologist*, vol. 24, no. 3, 2019, doi: 10.1634/theoncologist.2018-0177.
- [2] Rehman, A., Naz, S., Razzak, M. I., Akram, F., & Imran, M., “A Deep Learning-Based Framework for Automatic Brain Tumors Classification Using Transfer Learning,” *Circuits Syst Signal Process*, vol. 39, no. 2, 2020, doi: 10.1007/s00034-019-01246-3.
- [3] Lapointe, S., Perry, A., & Butowski, N. A. “Primary brain tumours in adults,” *The Lancet*, vol. 392, no. 10145, 2018. doi: 10.1016/S0140-6736(18)30990-5.
- [4] Van Maele-Fabry, G., Gamet-Payrastre, L., & Lison, D., “Residential exposure to pesticides as risk factor for childhood and young adult brain tumors: A systematic review and meta-analysis,” *Environment International*, vol. 106, 2017. doi: 10.1016/j.envint.2017.05.018.
- [5] Jones, D. T., Banito, A., Grünwald, T. G., Haber, M., Jäger, N., Kool, M., ... & Pfister, S. M. “Molecular characteristics and therapeutic vulnerabilities across paediatric solid tumours,” *Nature Reviews Cancer*, vol. 19, no. 8, 2019. doi: 10.1038/s41568-019-0169-x.
- [6] Miller, K. D., Ostrom, Q. T., Kruchko, C., Patil, N., Tihan, T., Cioffi, G., ... & Barnholtz- Sloan, J. S. “Brain and other central nervous system tumor statistics, 2021,” *CA Cancer J Clin*, vol. 71, no. 5, 2021, doi: 10.3322/caac.21693.
- [7] Cheng, J., Huang, W., Cao, S., Yang, R., Yang, W., Yun, Z., ... & Feng, Q. “Enhanced performance of brain tumor classification via tumor region augmentation and partition,” *PLoS One*, vol. 10, no. 10, 2015, doi: 10.1371/journal.pone.0140381.
- [8] Cheng, J., Yang, W., Huang, M., Huang, W., Jiang, J., Zhou, Y., ... & Chen, W. “Retrieval of Brain Tumors by Adaptive Spatial Pooling and Fisher Vector Representation,” *PLoS One*, vol. 11, no. 6, 2016, doi: 10.1371/journal.pone.0157112.
- [9] Charron, O., Lallement, A., Jarnet, D., Noblet, V., Clavier, J. B., & Meyer, P. “Automatic detection and segmentation of brain metastases on multimodal MR images with a deep convolutional neural network,” *Comput Biol Med*, vol. 95, 2018, doi: 10.1016/j.combiomed.2018.02.004.[10] Shao, L., Zhu, F., & Li, X., “Transfer learning for visual categorization: A survey,” *IEEE Trans Neural Netw Learn Syst*, vol. 26, no. 5, 2015, doi: 10.1109/TNNLS.2014.2330900.
- [11] Yang, Y., Yan, L. F., Zhang, X., Han, Y., Nan, H. Y., Hu, Y. C., ... & Wang, W., “Glioma grading on conventional MR images: A deep learning study with transfer learning,” *Front Neurosci*, vol. 12, no. NOV, 2018, doi: 10.3389/fnins.2018.00804.
- [12] Talo, M., Baloglu, U. B., Yildirim, Ö., & Acharya, U. R., “Application of deep transfer learning for automated brain abnormality classification using MR images,” *Cogn Syst Res*, vol. 54, 2019, doi: 10.1016/j.cogsys.2018.12.007.
- [13] Anaraki, A. K., Ayati, M., & Kazemi, F., “Magnetic resonance imaging-based brain tumor grades classification and grading via convolutional neural networks and genetic algorithms,” *Biocybern Biomed Eng*, vol. 39, no. 1, pp. 63–74, Jan. 2019, doi: 10.1016/j.bbe.2018.10.004.
- [14] Gumaei, A., Hassan, M. M., Hassan, M. R., Alelaiwi, A., & Fortino, G., “A Hybrid Feature Extraction Method with Regularized Extreme Learning Machine for Brain Tumor Classification,” *IEEE Access*, vol. 7, 2019, doi: 10.1109/ACCESS.2019.2904145.
- [15] Sajjad, M., Khan, S., Muhammad, K., Wu, W., Ullah, A., & Baik, S. W., “Multi-grade brain tumor classification using deep CNN with extensive data augmentation,” *J Comput Sci*, vol. 30, pp. 174–182, Jan. 2019, doi: 10.1016/j.jocs.2018.12.003.
- [16] Swati, Z. N. K., Zhao, Q., Kabir, M., Ali, F., Ali, Z., Ahmed, S., & Lu, J., “Brain tumor classification for MR images using transfer learning and fine-tuning,” *Computerized Medical Imaging and Graphics*, vol. 75, pp. 34–46, Jul. 2019, doi: 10.1016/j.compmedimag.2019.05.001.
- [17] Deepak, S., & Ameer, P. M., “Brain tumor classification using deep CNN features via transfer learning,” *Comput Biol Med*, vol. 111, 2019, doi: 10.1016/j.combiomed.2019.103345.
- [18] Alshayegi, M., Al-Buloushi, J., Ashkanani, A., & Abed, S. E., “Enhanced brain tumor classification using an optimized multi-layered convolutional neural network architecture,” *Multimed Tools Appl*, vol. 80, no. 19, pp. 28897–28917, Aug. 2021, doi: 10.1007/s11042-021-10927-8.
- [19] Kakarla, J., Isunuri, B. V., Doppalapudi, K. S., & Bylapudi, K. S. R., “Three- class classification of brain magnetic resonance images using average- pooling convolutional

- neural network,” *Int J Imaging Syst Technol*, vol. 31, no. 3, pp. 1731–1740, Sep. 2021, doi: 10.1002/ima.22554.
- [20] Kumar, R. L., Kakarla, J., Isunuri, B. V., & Singh, M., “Multi-class brain tumor classification using residual network and global average pooling,” *Multimed Tools Appl*, vol. 80, no. 9, pp. 13429–13438, Apr. 2021, doi: 10.1007/s11042-020-10335-4.
- [21] Ismael, M. R., & Abdel-Qader, I., “Brain Tumor Classification via Statistical Features and Back-Propagation Neural Network,” in *IEEE International Conference on Electro Information Technology*, 2018. doi: 10.1109/EIT.2018.8500308.
- [22] Abiwinanda, N., Hanif, M., Hesaputra, S. T., Handayani, A., & Mengko, T. R., “Brain tumor classification using convolutional neural network,” in *IFMBE Proceedings*, 2019. doi: 10.1007/978-981-10-9035-6_33.
- [23] Afshar, P., Plataniotis, K. N., & Mohammadi, A., “Capsule Networks for Brain Tumor Classification Based on MRI Images and Coarse Tumor Boundaries,” in *ICASSP, IEEE International Conference on Acoustics, Speech and Signal Processing - Proceedings*, 2019. doi: 10.1109/ICASSP.2019.8683759.
- [24] Afshar, P., Mohammadi, A., & Plataniotis, K. N., “Brain Tumor Type Classification via Capsule Networks,” in *Proceedings - International Conference on Image Processing, ICIP*, 2018. doi: 10.1109/ICIP.2018.8451379.
- [25] Abir, T. A., Siraji, J. A., Ahmed, E., & Khulna, B., “Analysis of a novel MRI based brain tumour classification using probabilistic neural network (PNN),” *Int. J. Sci. Res. Sci. Eng. Technol*, vol. 4, no. 8, pp. 65–79, 2018.
- [26] Chattopadhyay, A., & Maitra, M., “MRI-based brain tumor image detection using CNN based deep learning method,” *Neuroscience Informatics*, p. 100060, 2022.
- [27] Haq, A. U., Li, J. P., Khan, S., Alshara, M. A., Alotaibi, R. M., & Mawuli, C., “DACBT: deep learning approach for classification of brain tumors using MRI data in IoT healthcare environment,” *Sci Rep*, vol. 12, no. 1, 2022, doi: 10.1038/s41598-022-19465-1.
- [28] Cheng J., “Brain tumor dataset. Figshare. Dataset,” https://figshare.com/articles/dataset/brain_tumor_dataset/1512427, 2017.
- [29] Botta, B., Gattam, S. S. R., & Datta, A. K., “Eggshell crack detection using deep convolutional neural networks,” *J Food Eng*, vol. 315, p. 110798, 2022.
- [30] Thakur, S., & Kumar, A., “X-ray and CT-scan-based automated detection and classification of covid-19 using convolutional neural networks (CNN),” *Biomed Signal Process Control*, vol. 69, p. 102920, 2021.
- [31] Desale, R. P., & Verma, S. V., “Study and analysis of PCA, DCT & DWT based image fusion techniques,” in *2013 international conference on signal processing, image processing & pattern recognition*, IEEE, 2013, pp. 66–69.
- [32] Kumar, V., & Kumar, D., “A modified DWT-based image steganography technique,” *Multimed Tools Appl*, vol. 77, pp. 13279–13308, 2018.
- [33] Jana, D., & Sinha, K., “Wavelet thresholding for image noise removal,” *International Journal on Recent and Innovation Trends in Computing and Communication*, vol. 2, no. 6, pp. 1400–1405, 2014.
- [34] Lam, E. Y., & Goodman, J. W., “A mathematical analysis of the DCT coefficient distributions for images,” *IEEE transactions on image processing*, vol. 9, no. 10, pp. 1661–1666, 2000.
- [35] Parikh, R., Mathai, A., Parikh, S., Sekhar, G. C., & Thomas, R., “Understanding and using sensitivity, specificity and predictive values,” *Indian J Ophthalmol*, vol. 56, no. 1, p. 45, 2008.
- [36] Simonyan, K., & Zisserman, A., “Very deep convolutional networks for large-scale image recognition,” *arXiv preprint arXiv:1409.1556*, 2014.
- [37] Szegedy, C., Liu, W., Jia, Y., Sermanet, P., Reed, S., Anguelov, D., ... & Rabinovich, A., “Going deeper with convolutions,” in *Proceedings of the IEEE conference on computer vision and pattern recognition*, 2015, pp. 1–9.
- [38] He, K., Zhang, X., Ren, S., & Sun, J., “Deep residual learning for image recognition,” in *Proceedings of the IEEE conference on computer vision and pattern recognition*, 2016, pp. 770–778.
- [39] Howard, A. G., Zhu, M., Chen, B., Kalenichenko, D., Wang, W., Weyand, T., ... & Adam, H., “Mobilenets: Efficient convolutional neural networks for mobile vision applications,” *arXiv preprint arXiv:1704.04861*, 2017.